DE GRUYTER OPEN
DOI: 10.1515/ace-2015-0023
ARCHIVES OF CIVIL ENGINEERING
Vol. LXI ISSUE 3 2015

SHEAR LAG EFFECT IN THE NUMERICAL EXPERIMENT

M. SZUMIGAŁA[1], K. CIESIELCZYK[2]

The standard PN-EN 1993-1-5: 2008 (Eurocode 3) compared with the standard (PN-B-03200: 1990) used previously in Poland, introduces extended rules referring to the computations of the bearing capacity of the plated structural elements including the shear lag effect. The stress distribution in the width flanges is variable. Therefore in the case of the beam with the shear lag effect cannot be calculated by the classic beam theory.
In this article a comparison of the results of the calculations of forces distribution, stresses and displacement according to the rule presented in PN-EN 1993 and results of the numerical computations for 3D model (using finite element method) is presented. The elastic shear lag effects, the elastic shear lag effects including effects of the plate buckling and the elastic-plastic shear lag effects including the local instabilities were analysed. The calculations were performed for beams with a small and a large span and an influence of stiffeners was analysed.

Keywords: Eurocode 3, numerical analysis, plated structural elements, shear lag effect

1. INTRODUCTION

According to the classic beam theory the value of the normal stresses in the point with coordinates (x, y) is determined using the following formula:

$$\sigma_x = \frac{M_y}{I_y} z \; . \tag{1.1}$$

[1] DSc., PhD., Prof. Poznan University of Technology, Faculty of Civil Engineering and Environmental Engineering, Piotrowo 5, 60-965 Poznań, Poland, e-mail: maciej.szumigala@put.poznan.pl
[2] MSc, Poznan University of Technology, Faculty of Civil Engineering and Environmental Engineering, Piotrowo 5, 60-965 Poznań, Poland, e-mail: katarzyna.ciesielczyk@put.poznan.pl

This means that the distribution of the stresses in the y direction is constant on the entire width of the flange. However, when the flange of the beam becomes wider, this assumption becomes incorrect. The non-linear stress distribution occurs on the width of the flange in beams which have the width of the flanges larger than their length. This phenomenon is called the shear lag effect. The highest value of the stress in the flange occurs in the points situated directly above the web. The farther the point of the flange is away from the web, the value of the stress decreases (Fig. 1).

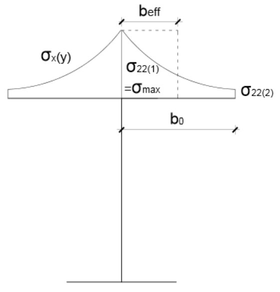

Fig. 1. Stress distribution in width flange [8]

Because of this phenomenon, in case of the beams with width flanges analysis , calculations cannot be performed according to the elementary theory of bending. Reducing the width of the flange to the effective width is assumed to be the simplest of the methods proposed in some design standards (also in Eurocode 3) [2].

2. IDEA IF THE EFFECTIVE WIDTH

The concept of the effective width was presented for the first time in 1924 by Theodore von Kármán [6] and it was related with effective width in relation to the thin-walled cross sections. Due to the simplicity of the proposed solution by Kármán it has been widely adopted to determine stress distribution due to shear lag in the steel structures.

It is assumed that the effective width is determined by the following formula:

(2.1) $$b_{eff} = \frac{1}{\sigma_{x,max}} \int_{0}^{b_0} \sigma_x(y)dy$$

where: b_{eff} – the effective width, $\sigma_{x,max}$ – the maximum value of the normal stress in the flange caused by of shear lag effect, $\sigma_x(y)$ – the normal stress in the flange, b_0 - the width of the flange, according to the Fig. 1.

In order to study the influence on the stress distribution of the shear lag effect the effective width factor β should be designated. The β ratio expresses the relation between the effective width and the real width [4]:

$$\beta = \frac{b_{eff}}{b_0}. \tag{2.2}$$

If the stress distribution in the flange is almost constant (shear lag effect is very small), the value of β ratio will be close to one. The bigger change of the stress distribution causes bigger influence of the shear lag effect (the of β ratio decreases). In the engineering practice often the stress distribution in the flange $\sigma_x(y)$ is unknown which should be determined. In this case, the effective width cannot be determined using the 2.1 formula. The effective width is determined by converting the 2.2 formula to:

$$b_{eff} = \beta b_0. \tag{2.3}$$

State of strains in the plates is determined by the following formula [5]:

$$\frac{\partial^2 \varepsilon_x}{\partial y^2} - \frac{\partial^2 \gamma}{\partial x \partial y} + \frac{\partial^2 \varepsilon_y}{\partial x^2} = 0 \tag{2.4}$$

where: ε_x –the strain in the longitudinal direction, ε_y – the strain in the transverse direction, γ – the shear strain.

In order to simplify the equation, it is assumed that the transverse stiffness is infinity (the strain in the transverse direction is equal to zero).

$$\frac{\partial \varepsilon_x}{\partial y} - \frac{\partial \gamma}{\partial x} = 0. \tag{2.5}$$

This assumption leads to the warping function w_s, which formula was presented by Johansson B et al. [3]. The final shape of the warping function is presented in the Figure 2. Strains are defined by the equations:

(2.6a) $$\varepsilon_x = -w_s \frac{\partial^2 \theta}{\partial x^2}$$

(2.6b) $$\gamma = -\frac{\partial w_s}{\partial y} \frac{\partial \theta}{\partial x}$$

where: θ – the angle of rotation.

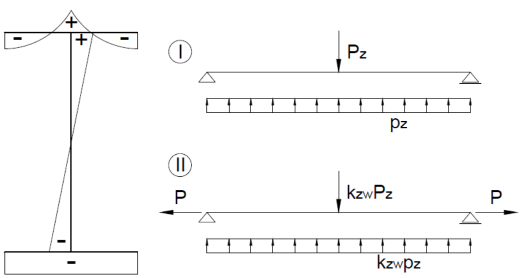

I: Hooke's law for bending:

(2.7) $$M_y = \frac{EI_y}{\rho}$$

where:

E – the Young's modulus, I_y – the moment of inertia with respect to the y axis: $I_y = \int z^2 dA$, A – the plane area, $\frac{1}{\rho}$ – the curvature: $\frac{1}{\rho} = w''$, w – the transverse displacement.

II:

(2.8) $$M_y' = EI_y' \frac{\partial^2 \theta}{\partial x^2} + P\theta$$

where:

$I_y' = \int w_s'^2 \, dA$,

$P = G \int \left(\frac{\partial w'}{\partial y} \right)^2 dA$.

Fig. 2. The final shape of the warping function [3]

In the next step the normal stress of the bending moment M_y (for the real width of the flange) and M_y' should be determined. The final stress distribution in width flange is formed by adding together these two stress values.

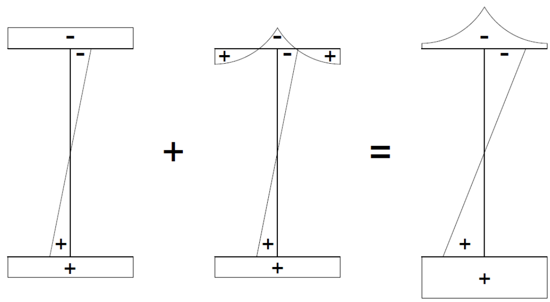

Fig. 3. Stress distribution with the shear lag effect [3]

The value of the effective width factor β depends on the shape of the bending moment diagram. To determine the β ratio formula the continuous beam should be divided into series of simple beams (the dividing points are these where the bending moment is zero). Then, depending on the shape of the bending moment at each of the beam parts the shape ratio ψ should be determined, by [3]:

(2.9)
$$\psi = 4\frac{\Delta M}{M_{max}}$$

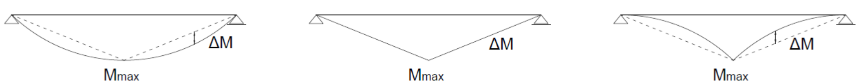

$$\Delta M = -\frac{M_{max}}{4} -> \psi = -1 \qquad \Delta M = 0 -> \psi = 0 \qquad \Delta M = \frac{M_{max}}{4} -> \psi = 1$$

Fig. 4. The shape ratio [5].

After solving the equation (2.4) and introducing some simplification (by [3]) the β ratio formula can be derived as follows:

(2.10)
$$\beta = \frac{1}{1 + 4(1+\psi)\frac{\alpha_0 b_0}{L_e} + 3{,}2(1-\psi)\left(\frac{\alpha_0 b_0}{L_e}\right)^2}$$

where: L_e – the effective width (the distance between adjacent points of zero bending moment), α_0 – the ratio depending on the cross section of the all longitudinal stiffeners, ΣA_{sl} – the area of all longitudinal stiffeners, t – the thickness of the flange.

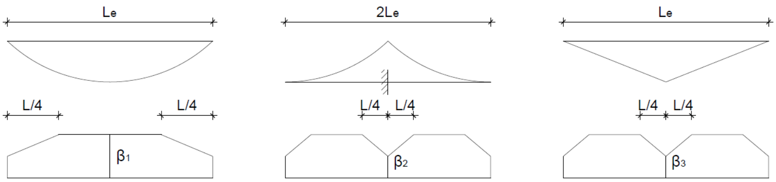

$$\beta_1 = \frac{1}{1 + 6{,}4\left(\frac{\alpha_0 b_0}{L}\right)^2} \qquad \beta_2 = \frac{1}{1 + 6\frac{\alpha_0 b_0}{L} + 1{,}6\left(\frac{\alpha_0 b_0}{L}\right)^2} \qquad \beta_3 = \frac{1}{1 + 4\frac{\alpha_0 b_0}{L} + 3{,}2\left(\frac{\alpha_0 b_0}{L}\right)^2}$$

Fig. 5. Effective width factor depending on the distribution of the bending moment [3]

The standard [8] includes ready formulas on the effective width factor β depending on the bending area.

3. Finite Element Model

In order to determine the forces and stress distribution, numerical computations in the Abaqus [10, 11] program were performed. The plated structural element was modelled as three – dimensional shell element. The steel beam was replaced by finite elements S4R – four – node shell elements with reduced integration (smaller number of Gauss points).

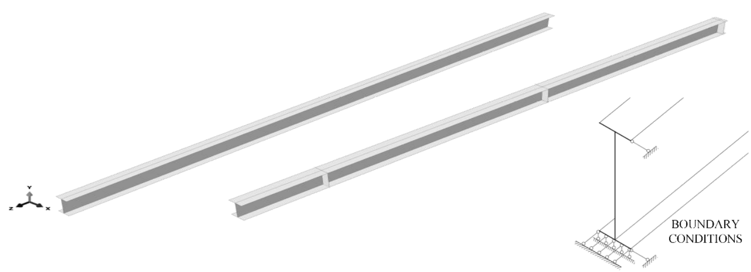

Fig. 6. Shell model of the plated structural element without and with the stiffeners

The loads were defined as distributed loads and applied to the entire length and width of the flange. The following two steel models were used in computations:

- Elastic model:
  - the Young's modulus: $E = 21 \cdot 10^{10} Pa$,
  - the Poisson's ratio: $\nu = 0{,}3$.

- Elastic – plastic model with minimal, linear strain hardening.

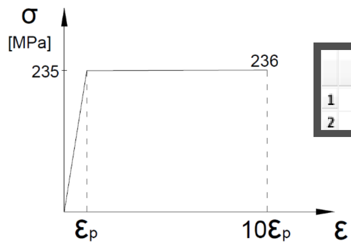

	Yield Stress	Plastic Strain
1	235000000	0
2	236000000	0.01

Fig 7. Elastic – plastic steel model with yielding plateau and minimal, linear strain hardening

The computations were performer using one of three computations procedures: *Static General* (elastic range analysis) and *Static Riks* and *Buckle* (elastic – plastic range analysis) in the Abaqus – Standard program.

4. THE RESULTS OF NUMERICAL ANALYSIS

The two – span beam with a cantilever in two variants of length was analysed. The first variant: large span – 12 m, with 4 m length cantilever, the second variant: small span – 6 m with 2 m length cantilever. The cross section depth is equal to 1/12 span. The distributed load 100 kN/m was applied on the entire length of the beam. In the computations the weight of the construction was omitted. According to the Eurocode 3 part 1 – 5 [8] it is obligatory to take into account the shear lag effect when the half width of the flange is less then effective length (the length between adjacent points of zero bending moment) divided by 50. The shear lag effect occurs for the chosen dimensions of the cross sections.

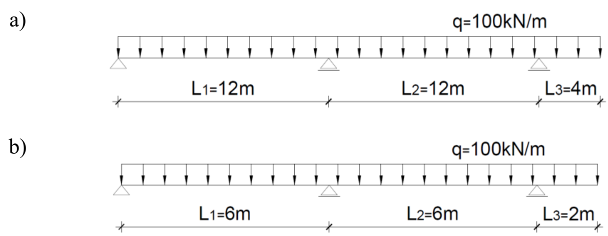

Fig. 8 The static scheme of the analysed beams: a) variant I, b) variant II

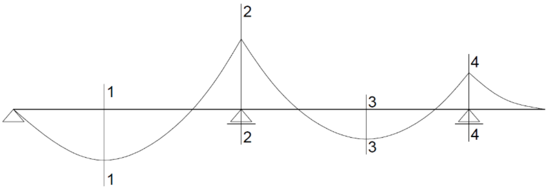

Fig. 9 Analysed sections

Firstly, calculations according to the norm EN 1993-1-5 [8] were performed, using the algorithm described in example given in [1]. Then, results were compared with the numerical computations performed by Abaqus. The aim of the task was to determine the shear forces and bending moments distribution in the beam with a wide flange. Then, the analysis of the stress distribution in the upper flange (in 2-2 and 4-4 sections) was performed.

4.1. ELASTIC SHEAR LAG EFFECT

Figure 10 presents the analysed cross sections dimensions in the elastic range. Table 1 presents the calculation steps needed to determine the effective width (according to the procedures of Eurocode 3 standard). To perform the numerical computations in the elastic range the *Static, General* procedure was used.

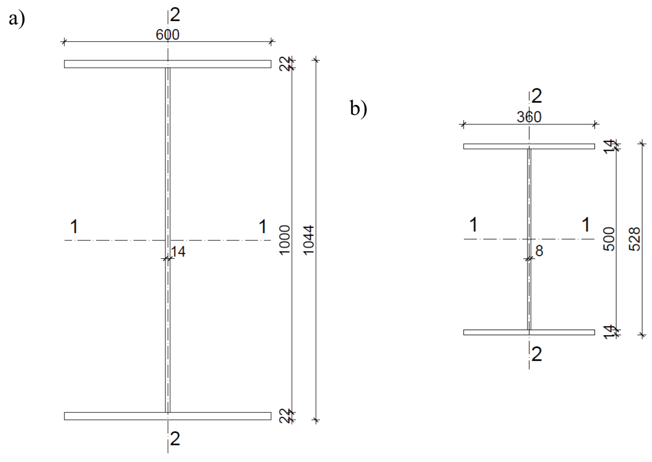

Fig. 10 The cross section of the analysed plated structural element: a) variant I, b) variant II

The beam with reduced stiffness was modelled in the program for bar structures computation (according to the scheme presented in the Figure 11). The determined values of the internal forces and stresses in characteristic sections were compared with the values from numerical analysis.
The comparison was performed in the Table 2 and 3.

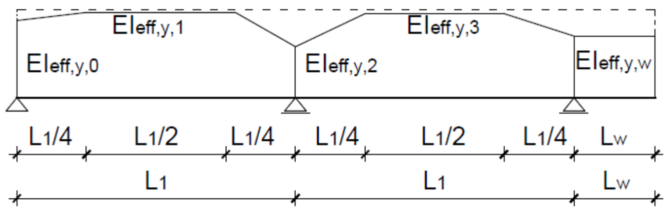

Fig. 11 The reduced stiffness of the cross section

Table 1. Effective width of the flange by [8]

Data		**Symbol**	**Unit**	**Large span**	**Small span**
Moment of inertia of the gross cross section		I_y	cm^4	806133	74927
Effective length		L_{e1}	m	10.2	5.1
		L_{e2}	m	6.0	3.0
		L_{e3}	m	8.4	4.2
		L_{e4}	m	8.0	4.0
Factor κ	end support	κ_0	-	0.0294	0,0353
	end span	κ_1	-	0.0294	0.0353
	middle support	κ_2	-	0.0500	0.0600
	middle span	κ_3	-	0.0357	0.0429
	cantilever	κ_w	-	0.0375	0.0450
Effective width factor	end support	β_0	-	0.994	0.992
	end span	β_1	-	0.994	0.992
	middle support	β_2	-	0.796	0.754
	middle span	β_3	-	0.992	0.992
	cantilever	β_w	-	0.860	0.820
Effective width of the flange	end support	$b_{eff,0}$	mm	597	357
	end span	$b_{eff,1}$	mm	597	357
	middle support	$b_{eff,2}$	mm	478	272
	middle span	$b_{eff,3}$	mm	595	356
	cantilever	$b_{eff,w}$	mm	516	295
Moment of inertia of the net cross section		$I_{eff,y,0}$	cm^4	802685	74372
		$I_{eff,y,1}$	cm^4	802685	74372
		$I_{eff,y,2}$	cm^4	665941	58649
		$I_{eff,y,3}$	cm^4	800387	74187
		$I_{eff,y,w}$	cm^4	709607	62903
All symbols which are included in this table are the symbols from Eurocode 3 [8]					

Table 2. Internal forces

Data	Cross section	Unit	Large span			Small span		
			Analytical results		Numerical results	Analytical results		Numerical results
			Gross cross section	Net cross section		Gross cross section	Net cross section	
Bending moment	1-1	kNm	1088.9	1113.6	1088.9	272.2	280.1	277.7
	2-2	kNm	1600.0	1536.9	1600.0	400.0	378.0	381.8
	3-3	kNm	622.2	650.4	622.2	155.6	164.5	162.2
	4-4	kNm	800.0	800.0	800.0	200.0	200.0	198.0
Shear force	2-2 (left)	kN	733.3	728.1	733.3	366.7	363.3	359.2
	2-2 (right)	kN	666.7	661.4	666.7	333.3	330.0	329.3
	4-4 (left)	kN	533.3	538.6	533.3	266.7	270.0	264.2
	4-4 (right)	kN	400.0	400.0	400.0	200.0	200.0	198.6

Table 3. Stress values in the upper flange

Section		Large span			Small span		
		Stress [MPa]		Percentage difference*	Stress [MPa]		Percentage difference*
		Analytical results	Numerical results		Analytical results	Numerical results	
2-2	Max. stress	120.5	126.0	4.4 %	170.2	174.1	2.2 %
	Min. stress	89.8	91.8	2.2 %	117.9	124.5	5.3 %
4-4	Max. stress	58.8	72.8	19.2 %	83.9	106.9	21.5 %
	Min. stress	48.6	46.0	5.7 %	65.0	63.1	3.0 %

*Percentage difference is the numerical minus analytical result divided by the value of numerical result.

Additionally the influence of stiffeners on the stress distribution in the width flanges was analysed. The beams calculated above were modelled using the stiffeners. The comparison of the results in the table below was performed.

Table 4. The value of the stress in beam with and without stiffeners

Cross section		Large span		Small span	
		Stress [MPa]		Stress [MPa]	
		Without stiffeners	With stiffeners	Without stiffeners	With stiffeners
2-2	Max. stress	126.0	101.4	174.1	135.3
	Min. stress	91.8	92.8	124.5	116.1
4-4	Max. stress	72.8	54.6	106.9	73.0
	Min. stress	46.0	46.4	63.1	62.0

4.2. COMBINED EFFECTS OF SHEAR LAG AND PLATE BUCKLING

In the next step of the combined effects of shear lag and plate buckling were analysed. The first cross section of the flange was reduced from 22 to 14 mm and the second cross section was reduced from 14 to 10 mm in order to classify them to the 4 class.

To perform the calculations in elastic range with effects of plate buckling the *Static, General* procedure with geometrical nonlinearity was used.

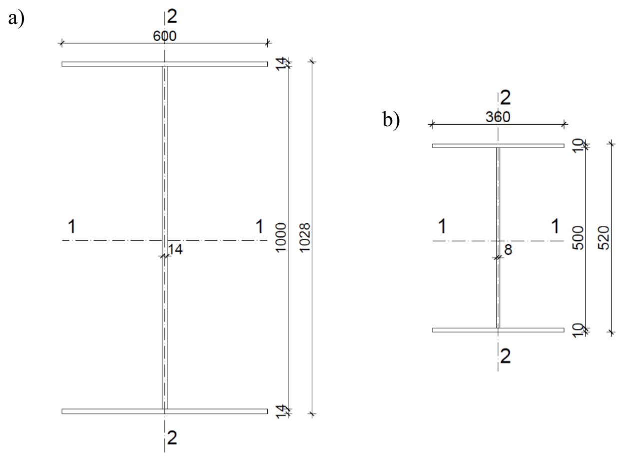

Fig. 12. The cross section of the analysed plated structural element: a) variant I, b) variant II

Table 5. Effective width of the flange [8]

Data		Symbol	Unit	Large span	Small span
Moment of inertia of the gross cross section		I_y	cm^4	488075	55157
Factor κ	end support	κ_0	-	0.035	0.046
	end span	κ_1	-	0.035	0.046
	middle support	κ_2	-	0.060	0.077
	middle span	κ_3	-	0.043	0.055
	cantilever	κ_w	-	0.045	0.058
Effective width factor	end support	β_0	-	0.992	0.987
	end span	β_1	-	0.992	0.987
	middle support	β_2	-	0.753	0.693
	middle span	β_3	-	0.988	0.981
	cantilever	β_w	-	0.992	0.762
Effective width of the compression flange	end support	$b_{eff,0}$	mm	432	296
	end span	$b_{eff,1}$	mm	432	296
	middle support	$b_{eff,2}$	mm	328	208
	middle span	$b_{eff,3}$	mm	431	294
	cantilever	$b_{eff,w}$	mm	358	229
Effective width of the tension flange	end support	$b_{eff,0}$	mm	595	355
	end span	$b_{eff,1}$	mm	595	355
	middle support	$b_{eff,2}$	mm	452	249
	middle span	$b_{eff,3}$	mm	593	353
	cantilever	$b_{eff,w}$	mm	492	274
Moment of inertia of the net cross section		$I_{eff,y,0}$	cm^4	481558	50455
		$I_{eff,y,1}$	cm^4	481558	50455
		$I_{eff,y,2}$	cm^4	394273	37926
		$I_{eff,y,3}$	cm^4	480529	50194
		$I_{eff,y,w}$	cm^4	419082	40899
All symbols which are included in this table are the symbols from Eurocode 3 [8].					

Table 6. Internal forces

Data	Cross section	Unit	Large span			Small span		
			Analytical results		Numerical results	Analytical results		Numerical results
			Gross cross section	Net cross section		Gross cross section	Net cross section	
Bending moment	1-1	kNm	1088.9	1114.2	1103.0	272.2	281.5	277.0
	2-2	kNm	1600.0	1535.2	1562.0	400.0	376.3	385.8
	3-3	kNm	622.2	651.1	638.4	155.6	166.2	161.1
	4-4	kNm	800.0	800.0	797.5	200.0	200.0	198.4
Shear force	2-2 (left)	kN	733.3	727.9	727.9	366.7	362.7	364.7
	2-2 (right)	kN	666.7	661.3	659.5	333.3	329.4	329.5
	4-4 (left)	kN	533.3	538.7	535.4	266.7	270.6	268.4
	4-4 (right)	kN	400.0	400.0	396.0	200.0	200.0	198.0

Table 7. Stress values in the upper flange

Cross section		Large span			Small span		
		Stress [MPa]		Percentage difference	Stress [MPa]		Percentage difference
		Without stiffeners	With stiffeners		Without stiffeners	With stiffeners	
2 - 2	Max. stress	186.5	207.5	10.1 %	246.0	253.3	2.9 %
	Min. stress	128.9	130.0	0.8 %	151.6	163.7	7.4 %
4 - 4	Max. stress	91.1	134.5	32.3 %	120.8	161.6	25.2 %
	Min. stress	70.6	64.4	9.6 %	84.6	81.1	4.3 %
*Percentage difference is the numerical minus analytical result divided by the value of numerical result.							

In the table 5 the data needed for analytical computations according to the Eurocode 3 [8] were presented. The in the tables 6 and 7 the comparison of the analytical and numerical results (the values of internal forces and the stress values) was shown. The difference between the values of the stress is smaller in the case of minimal stress then in the case of maximum stress (in the web axis).

4.3. ELASTIC – PLASTIC SHEAR LAG EFFECT

The last step of the analysis included the combined effects of elastic – plastic shear lag effect with limited plastic strains and of plate buckling. The beams as in subsection 4.2 with elastic – plastic model of steel were analysed. This type of analysis was also presented in [7]. In order to determine the limit load for class 4 cross sections in elastic – plastic range the two types of analysis: *Buckle* and *Static Riks* ware used. The first type of analysis – *Buckle* – is used to determine the form of the stability loss . Then, the *Static Riks* analysis which takes into account the geometric imperfections were performed. The results from the first analysis were scaled, so imperfections do not exceed the limit values, according to the standard [9]. Then, the obtained values were loaded to the *Static Riks* procedure.

The beams were divided into sections on the entire width of the flange with a value of 100 kN/m^2. The load increase (from the chart LPF – *Load Proportionality Factor*) was observed during *Static*

Riks analysis. When this function has reached the maximum value and the load started to decrease the loss of stability and bearing capacity occurred. The value of maximum load was read from the LPF diagram and for this value the analytical calculations according to the standard [8] were performed.

a) b)

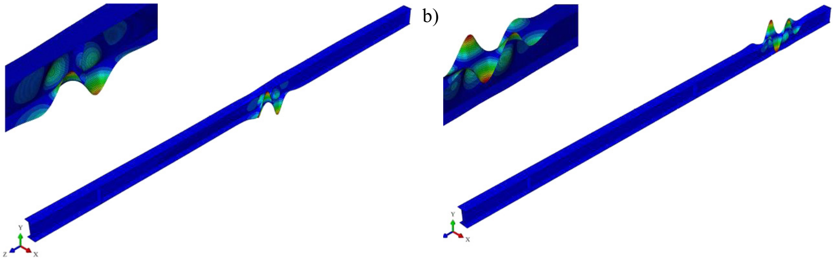

Fig. 13. The mode illustrating forms of the local loss of stability: a) first form, b) second form.

a)

b)

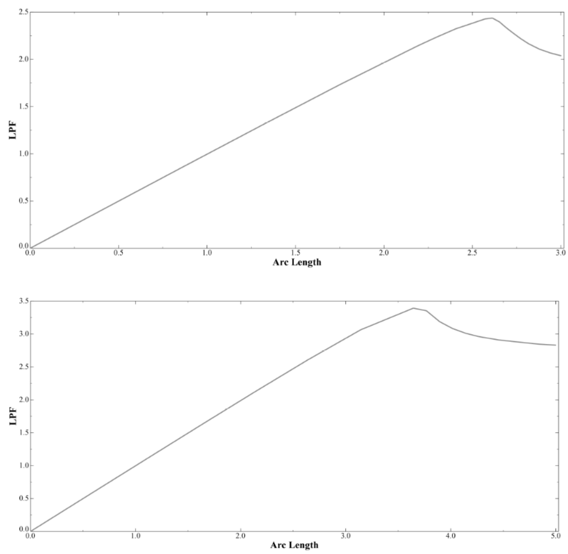

Fig. 14. Load proportionality factor: a) variant I (LPF=2.438), b) variant II (LPF=3.393).

Table 8. Effective width of the flange [8]

Data		Symbol	Unit	Large span	Small span
Effective width of the compression flange	end support	beff,0	mm	436	300
	end span	beff,1	mm	436	300
	middle support	beff,2	mm	429	292
	middle span	beff,3	mm	436	300
	cantilever	beff,w	mm	432	292
Effective width of the tension flange	end support	beff,0	mm	600	360
	end span	beff,1	mm	600	360
	middle support	beff,2	mm	590	350
	middle span	beff,3	mm	600	360
	cantilever	beff,w	mm	595	354
Moment of inertia of the net cross section		Ieff,y,0	cm4	488942	51035
		Ieff,y,1	cm4	488942	51035
		Ieff,y,2	cm4	478776	49875
		Ieff,y,3	cm4	484760	51035
		Ieff,y,w	cm4	487558	50324
All symbols which are included in this table are the symbols from Eurocode 3 [8].					

Table 9. Internal forces

Data	Cross section	Unit	Large span			Small span		
			Analytical results		Numerical results	Analytical results		Numerical results
			Gross cross section	Net cross section		Gross cross section	Net cross section	
Bending moment	1-1	kNm	1088.9	1593.6	1624.0	272.2	332.7	343.6
	2-2	kNm	1600.0	2339.1	2228.0	400.0	486.4	456.9
	3-3	kNm	622.2	911.1	949.2	155.6	190.8	202.5
	4-4	kNm	800.0	1170.4	1159.0	200.0	244.2	241.7
Shear force	2-2 (left)	kN	733.3	1072.2	1034.0	366.7	447.4	434.8
	2-2 (right)	kN	666.7	975.2	937.2	333.3	406.7	394.0
	4-4 (left)	kN	533.3	780.4	772.8	266.7	325.9	326.1
	4-4 (right)	kN	400.0	585.2	517.5	200.0	244.2	240.3

Table 9. Internal forces

Data	Cross section	Unit	Large span			Small span		
			Analytical results		Numerical results	Analytical results		Numerical results
			Gross cross section	Net cross section		Gross cross section	Net cross section	
Bending moment	1-1	kNm	1088.9	1593.6	1624.0	272.2	332.7	343.6
	2-2	kNm	1600.0	2339.1	2228.0	400.0	486.4	456.9
	3-3	kNm	622.2	911.1	949.2	155.6	190.8	202.5
	4-4	kNm	800.0	1170.4	1159.0	200.0	244.2	241.7
Shear force	2-2 (left)	kN	733.3	1072.2	1034.0	366.7	447.4	434.8
	2-2 (right)	kN	666.7	975.2	937.2	333.3	406.7	394.0
	4-4 (left)	kN	533.3	780.4	772.8	266.7	325.9	326.1
	4-4 (right)	kN	400.0	585.2	517.5	200.0	244.2	240.3

a)

b)

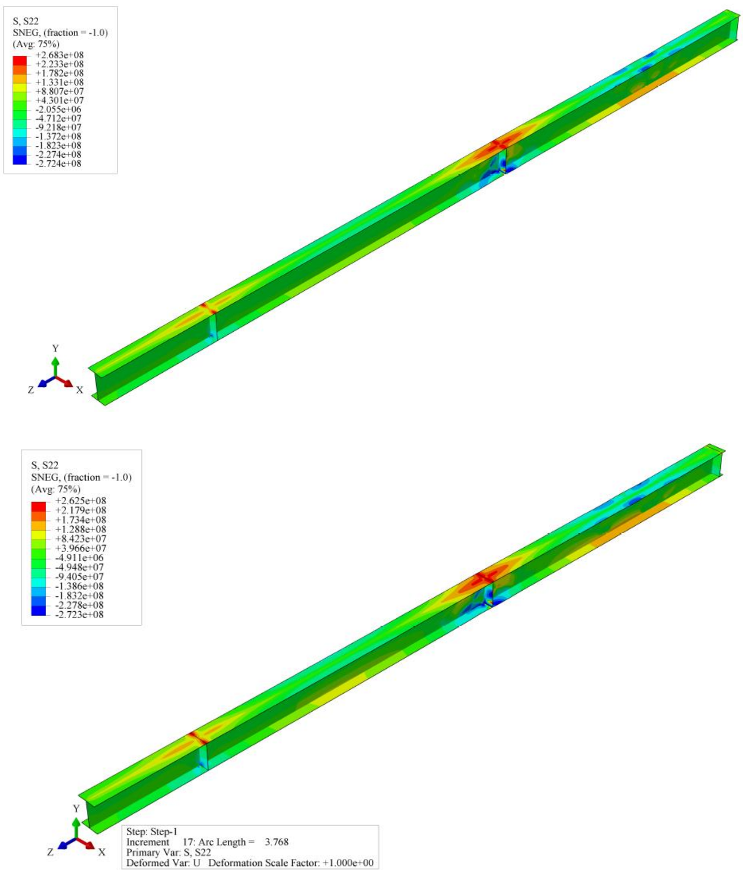

Fig. 15. The normal stress map corresponding to the Mises stress equal 236 MPa [Pa]:
a) large span beam, b) small span beam.

5. CONCLUSIONS

The results and analysis of the performed analytical and numerical calculations led to the following conclusion:

1° It was proven that internal forces in beams with wide flanges cannot be calculated according to the elementary theory of bending. In statically indeterminate beams the values of bending moments and shear forces depend on the width of the flange.

2° The calculation method of the internal forces in beams presented in Eurocode 3 gives similar results to the results obtained in the numerical analysis (using Abaqus program). The percentage difference between the analytical and numerical results (in the examples presented in this article) is presented in the table.

Table 10. The percentage difference between presented results

Data	Elastic analysis without plate buckling	Elastic analysis taking into account the effect of plate buckling	Elastic – plastic analysis taking into account the effect of plate buckling
Bending moment	0.5 – 1.5 %	0.4 – 2.0%	1.0 – 5.0 %
Shear force	0.5 – 2.0%	0.0 – 1.0%	1.0 – 2.0%

3° The shear lag effects influence the change of internal forces distribution. Therefore, the static calculation (not only in determining the bearing capacity) must take into account the reduced stiffness of the cross section.

4° It was proven that using the numerical computations for the beam with width flanges, the stress values cannot be determined using the classic beam theory, ($\sigma_x = \frac{M_y}{I_y} z$) because the stress distribution in the flange is not constant. The maximum value of the stress is in the web axis and minimal on the edge of the flange. The decrease of the stress distribution describes the non – linear function. It can be concluded that the function equation given in Eurocode 3 gives results consistent with the results obtained in the numerical analysis.

5° The shear lag effect is more evident in shorter beams. This means that the value of the effective width factor β increases with increasing the span of the beam.

6° The use of stiffeners reduces the effect of non-linear stress distribution in the wide flange. The maximum stress $\sigma_{22(1)}$ in the web axis may be lowered by using stiffeners (about 26% for middle support and 46% for support next to the cantilever). However, the minimum stress $\sigma_{22(2)}$ on the edge of the flange may increase or decrease about 5%. Therefore, the difference between maximum and minimum values of the stress are lowered by using the stiffeners (the lower influence of shear lag effect).

REFERENCES

1. Goczek J., Supeł Ł., Gajdzicki M., Przykłady obliczeń konstrukcji stalowych, Lodz University of Technology, Poland, 2010
2. Jankowiak R., Elementy smukłościenne (blachownice) – obliczenia i kształtowanie, XXVII Ogólnopolskie warsztaty pracy projektanta konstrukcji, Szczyrk, marzec 2012
3. Johansson B., Maquoi R., Sedlacek G., Müller C., Beg D. Commentary and worked examples to EN 1993-1-5 Plated structuralelements, JRC Scientific and Technical Raports, First Edition, October 2007
4. Sa – nguanmanasak J., Stress concentration due to shear lag in simply supported box girders with longitudinal stiffeners and continuous box girders and finite element modeling of steel – Concrete composite bridge, Sirindhorn International Institute of Technology, Thammasat University, Thailand, May 2010
5. Sørensen R. K., Evaluation of shear lag in standard H-/I-sections, Aalborg University Esbjerg, Denmark, 2013
6. Kármán, Th. Von, The effective width (in German), Beitrage zur technischen Mechanik, p. 114-127, Springer-Verlag Berlin Heidelberg Gmbh, German, 1924
7. Piekarczyk M., Wykorzystanie nadkrytycznej rezerwy nośności w projektowaniu konstrukcji stalowych, Tadeusz Kosciuszko Cracow University of Technology, Poland, 2002
8. EN 1993-1-5, Eurocode 3, Design of steel structures – Part 1-5 Plated structural elements, 2006
9. PN-EN 1090-2, Wykonywanie konstrukcji stalowych i aluminiowych, Część 2: Wymaganie techniczne dotyczące konstrukcji stalowych, 2012
10. Abaqus 6.10 Documentation, *"Abaqus/CEA User's Manual"*.
11. Abaqus 6.10 Documentation, *"Abaqus Analysis User's Manual"*.

Received 04. 12. 2014
Revised 12. 02. 2015

LIST OF FIGURES AND TABLES:

Fig. 10. The cross section of the analysed plated structural element: a) variant I, b) variant II

Rys. 10. Przekrój analizowanej blachownicy: a) wariant I, b) wariant II

Fig. 11. The reduced stiffness of the cross section

Rys. 11. Zredukowana sztywność przekroju

Fig. 12. The cross section of the analysed plated structural element: a) variant I, b) variant II

Rys. 12. Przekrój analizowanej blachownicy: a) wariant I, b) wariant II

Fig. 13. The mode illustrating forms of the local loss of stability: a) first form, b) second form

Rys. 13. Moda ilustrująca postacie lokalnej utraty stateczności: a) pierwsza postać, b) druga postać

Fig. 14. Load proportionality factor: a) variant I (LPF=2.438), b) variant II (LPF=3.393)

Fig. 15. The normal stress map corresponding to the Mises stress equal 236 MPa [Pa]: a) large span beam, b) small span beam

Rys. 15. Mapy naprężeń normalnych odpowiadających naprężeniom Misesa równym 236 MPa [Pa]: a) belka o dużej rozpiętości, b) belka o małej rozpiętości

Tab. 1. Effective width of the flange by [8]

Tab. 1. Szerokość efektywna pasa wg [8]

Tab. 2. Internal forces

Tab. 2. Siły wewnętrzne

Tab. 3. Stress values in the upper flange

Tab. 3. Wartości naprężeń w pasie górnym

Tab. 4. The value of the stress in beam with and without stiffeners

Tab. 4. Wartości naprężeń w belce bez i z żeberkami usztywniającymi

Tab. 5. Effective width of the flange by [8]

Tab. 5. Szerokość efektywna pasa wg [8]

Tab. 6. Internal forces

Tab. 6. Siły wewnętrzne

Tab. 7. Stress values in the upper flange

Tab. 7. Wartości naprężeń w pasie górnym

Tab. 8. Effective width of the flange by [8]

Tab. 8. Szerokość efektywna pasa wg [8]

Tab. 9. Internal forces

Tab. 9. Siły wewnętrzne

Tab. 10. The percentage difference between presented results

Tab. 10. Różnica procentowa pomiędzy wynikami

EFEKT „SZEROKIEGO PASA" W EKSPERYMENCIE NUMERYCZNYM

Słowa kluczowe: Eurokod 3, analiza numeryczna, blachownice, efekt szerokiego pasa

STRESZCZENIE:

Norma PN-EN_1993-1-5: 2008 (Eurocode 3) w porównaniu do dotychczas obowiązującej w Polsce normie dotyczącej projektowania konstrukcji stalowych (PN-B-03200: 1990) wprowadza rozszerzone zasady obliczania nośności konstrukcji blachownicowych o uwzględnianie efektu „szerokiego pasa". Rozkład naprężeń w szerokich pasach jest zmienny i z tego powodu w przypadku belek podlegających efektowi szerokiego pasa nie można przeprowadzać obliczeń według klasycznej teorii belkowej.

W artykule można wyróżnić dwie główne części: pierwszą zawierającą wstęp oraz teoretyczny opis podstaw dotyczących szerokości efektywnej i efektu szerokiego pasa (rozdziały pierwszy i drugi) oraz drugą przedstawiającą wyniki obliczeń analitycznych i numerycznych wpływu efektu szerokiego pasa na rozkład sił wewnętrznych (rozdziały trzeci i czwarty). W rozdziale piątym przedstawione zostały wnioski z przeprowadzonych analiz.

W części pierwszej – opisie teoretycznym odniesiono się do pojęcia szerokości efektywnej, która po raz pierwszy została zaprezentowana przez Kármána w 1924 roku. Następnie podano definicję współczynnika β, który określa wpływ efektu „szerokiego pasa" dla różnych schematów rozkładu momentu zginającego. Przedstawione w artykule wyprowadzenia stanowią podstawę dla gotowych wzorów na uwzględnienie efektu „szerokiego pasa" w projektowaniu elementów stalowych zaprezentowanych w normie EN-1993-1-1.

W drugiej części artykułu przedstawiono obliczenia sił wewnętrznych, rozkładu naprężeń oraz przemieszczeń według zasad zawartych w EN 1993-1-1. Obliczenia przeprowadzono dla belek dwuprzęsłowych z częścią wspornikową (o długości 2 m) o małej rozpiętości (6 m) oraz dużej rozpiętości (12 m) przęsła. Wysokość przekroju poprzecznego blachownicy przyjęto równą 1/12 rozpiętości przęsła. Założono obciążenie równomiernie rozłożone na całej długości belki równe 100 kN/m. W obliczeniach pomięto ciężar własny konstrukcji. Przeprowadzone obliczenia podzielono na trzy grupy:

1) analizę efektu „szerokiego pasa" w zakresie sprężystym;
2) analizę efektu „szerokiego pasa" w zakresie sprężystym z uwzględnieniem wpływu lokalnej utraty stateczności;
3) analizę efektu „szerokiego pasa" w zakresie sprężysto – plastycznym.

Wyniki otrzymane w wyniku obliczeń analitycznych (zgodnie z normą) porównano z wynikami przeprowadzonej analizy numerycznej (przy użyciu metody elementów skończonych). Stworzono powłokowy, przestrzenny model blachownicy z elementów skończonych typu S4R o wymiarze 2 x 2 mm. Do obliczeń numerycznych wykorzystano program Abaqus CEA.

W pierwszej grupie obliczeniowej przedstawiono analizę efektu szerokiego pasa jedynie w zakresie sprężystym. Na tym etapie obliczeń analizowano przekroje klasy pierwszej, czyli nieulegające lokalnej utracie stateczności.

Druga grupa obliczeniowa obejmowała przekroje klasy czwartej, ale analiza prowadzona była również tylko w zakresie sprężystym – obliczenia zawierają złożone efekty szerokiego pasa oraz niestateczności ścianki. Do porównania wyników analitycznych w zakresie sprężystym, w obliczeniach numerycznych wykorzystano procedurę obliczeniową typu *Static, General*.

W ostatniej grupie obliczeniowej przedstawiono obliczenia złożonych efektów szerokiego pasa i niestateczności ścianki w zakresie sprężysto – plastycznym. Wykorzystano normowy, sprężysto – plastyczny model stali z minimalnym,

liniowym wzmocnieniem. W tym przypadku obliczenia numeryczne zostały podzielone na dwa etapy. Pierwszy z nich obejmował analizę *Buckle* w celu znalezienia kolejnych postaci utraty stateczności analizowanego modelu. Następnie, w drugim etapie wyniki z analizy *Buckle* zostały wczytane do modelu jako wstępne imperfekcje geometryczne. Wyniki zostały przeskalowane w taki sposób, by nie zostały przekroczone graniczne wartości imperfekcji zgodnie z normą PN-EN 1090-2. Drugi etap analizy został przeprowadzony przy wykorzystaniu procedury *Static, Ricks* dzięki której znaleziona została graniczna wartość obciążenia, po przekroczeniu której element ulegał utracie stateczności.

Przeprowadzone analizy wykazały, że siły wewnętrzne w belkach z szerokim pasem nie mogą być wyznaczane zgodnie z klasyczną teorią zginania, ponieważ wartości momentu zginającego oraz sił ścinających zależą od szerokości pasa. Wynika z tego, że w obliczeniach statycznych należy uwzględnić zredukowaną sztywność przekroju w odpowiednich przekrojach charakterystycznych na długości belki.

Przeprowadzone obliczenia numeryczne udowodniły również, że naprężenia w szerokich pasach nie mogą być wyznaczane zgodnie z klasyczną teorią belkową, ponieważ ich rozkład na szerokości pasa nie jest stały – maksymalne wartości naprężeń występują w przekroju nad środnikiem, a minimalne na krawędziach zewnętrznych pasa.

Warto również wspomnieć, że zapisy normowe dotyczących wpływu efektu „szerokiego pasa" nie prezentują w jaki sposób uwzględnić wpływ żeberek podporowych na rozkład naprężeń w pasach. Z uwagi na fakt, że w blachownicowych konstrukcjach stalowych żeberka podporowe są bardzo często stosowane, autorzy uznali za zasadne sprawdzenie jak zmieni się rozkład naprężeń w szerokim pasie po zastosowaniu żeberek. Z tego powodu w przeanalizowanych już modelach numerycznych dodano żeberka podporowe i porównano wyniki. Okazało się, że dodanie żeberek podporowych redukuje efekt „szerokiego pasa". Zastosowanie żeberek spowodowało redukcję naprężeń w przekroju w osi środnika na poziomie 45%, a praktycznie zerową redukcję w przekroju na końcu pasa – co spowodowało zredukowanie nieliniowego rozkładu naprężeń w szerokim pasie.